Published in "Journal of Physics: Condensed Matter 23(3): 036002, 2011"
which should be cited to refer to this work.

Magnetic and electronic properties of $RNiO_3$ (R = Pr, Nd, Eu, Ho and Y) perovskites studied by resonant soft x-ray magnetic powder diffraction

Y Bodenthin[1], U Staub[1], C Piamonteze[1], M García-Fernández[1,2], M J Martínez-Lope[3] and J A Alonso[3]

[1] Swiss Light Source, Paul Scherrer Institut, CH-5232 Villigen PSI, Switzerland
[2] Institut de Physique, Université de Fribourg, CH-1700 Fribourg, Switzerland
[3] Instituto de Ciencia de Materiales de Madrid, CSIC, Cantoblanco, E-28049 Madrid, Spain

E-mail: urs.staub@psi.ch

Abstract

Soft x-ray resonant magnetic powder diffraction of the $(\frac{1}{2}\ 0\ \frac{1}{2})$ reflection at the Ni $L_{2,3}$ edges is used to study the magnetic and electronic properties of a series of $RNiO_3$ materials (with R = Pr, Nd, Eu, Ho and Y) below the metal–insulator transition. The polarization and energy dependence of the reflection gives further support for a non-collinear magnetic structure and charge disproportionation in the whole $RNiO_3$ series. Only small changes in the spectra of the magnetic $(\frac{1}{2}\ 0\ \frac{1}{2})$ reflection and in the absorption spectra could be detected. The results are discussed with comparison to charge transfer multiplet calculations. Our results emphasize that the lighter and heavier $RNiO_3$ compounds are very similar from the point of view of their local electronic and magnetic state despite the strong change of the metal-to-insulator transition temperature.

1. Introduction

Transition metal oxides with perovskite structure show an interesting ensemble of physical properties due to the tight relationship between lattice, charge, orbital, and magnetic degrees of freedom. The interplay and competition between different degrees of freedom can lead to charge and orbital ordered ground states for which the electrons are localized. These systems often show metal-to-insulator transitions, whose microscopic origin is of ongoing interest [1]. The rare earth nickel perovskites ($RNiO_3$, R = rare earth ion or Y) present a sharp, well-defined metal-to-insulator (MI) transition [2] where the transition temperature T_{MI} depends on the ionic radius of the R ion [3]. For small R ions, T_{MI} exceeds the antiferromagnetic ordering temperature, T_N, and for larger R ions (except La), T_{MI} and T_N coincide.

$RNiO_3$ materials crystallize in the orthorhombic distorted perovskite structure with *Pbnm* symmetry and unit cell dimensions $\sqrt{2}a_p \times \sqrt{2}a_p \times 2a_p$, where a_p is the simple perovskite lattice parameter. The nominal valence of Ni is 3+ with d-electron figuration $t_{2g}^6 e_g^1$ and spin $S = \frac{1}{2}$. $RNiO_3$ has a small or even negative charge transfer energy and theoretical considerations favor a charge ordered rather than orbital ordered state below T_{MI} [4, 5]. In the $RNiO_3$ series, $LaNiO_3$ has the largest one-electron bandwidth and remains metallic. All other $RNiO_3$ compounds have an insulating ground state, i.e. they exhibit a first order metal-to-insulator transition at T_{MI} and if $T_N \neq T_{MI}$ a further second order transition to long-range antiferromagnetic order with $T_N \leqslant T_{MI}$. Values of T_{MI} and the Néel temperatures for $RNiO_3$ with R ions investigated in this study are given in table 1. High-resolution x-ray powder diffraction experiments found that the strongly distorted members of the $RNiO_3$ series (e.g. $YNiO_3$) have a charge ordered ground state of the type $2Ni^{3+} \rightarrow Ni^{3+\delta}/Ni^{3-\delta}$ (charge disproportionation) [6–8], occurring

Table 1. Metal-to-insulator transition temperatures, T_{MI} (K), Néel temperatures, T_N (K), tolerance factors, t, and branching ratios for $RNiO_3$ perovskites. Data taken from [6, 20, 29, 30, 33, 34].

R	T_{MI}	T_N	t	Branching ratio
Pr	130	130	0.925	0.973 ± 0.004
Nd	200	200	0.915	0.970 ± 0.005
Eu	462.5	205	0.887	0.977 ± 0.005
Ho	572.9	145	0.866	0.978 ± 0.003
Y	582.1	145	0.864	0.982 ± 0.005

at the metal-to-insulator transition. This interpretation is based on the observed symmetry lowering to a monoclinic $P2_1/n$ crystal structure ($\beta = 90.08°$) at $T < T_{MI}$, which breaks up the single Ni site in the metallic phase into two individual crystallographic sites. Resonant x-ray diffraction [9, 10] and Raman spectroscopy [11] studies indicate that a disproportionation also occurs for the larger Nd ion. The data show that for $T < T_{MI}$ the $Pbnm$ symmetry is lowered to $P2_1/n$ [9, 12]. More recent x-ray absorption measurements and high-resolution neutron powder diffraction on R = Pr materials also reveal charge ordering below T_{MI} [13, 14]. It is predicted that the centrosymmetric space group $P2_1/n$ and charge ordering (CO) leads to multiferroic behavior [15–17]. High-resolution x-ray absorption measurements reveal a distinct, rare-earth-dependent splitting of the Ni K edge throughout the whole $RNiO_3$ perovskite family. The results were interpreted in terms of significant changes in charge disproportionation, with a small degree of disproportionation for $RNiO_3$ with low T_{MI} and a large degree for the end member of the lanthanides with high T_{MI} [18].

Different models for the magnetic structure based on neutron powder diffraction data [6, 19, 20] have been discussed, but due to the lack of sizable single crystals, the magnetic structure remains ambiguous. From the magnetic structure characterized by a $(\frac{1}{2}\ 0\ \frac{1}{2})$ wavevector, an up–up–down–down stacking of Ni magnetic moments was proposed [19], which implies an orbital ordering scenario for the Ni e_g orbitals. Nevertheless, orbital ordering is inconsistent with charge disproportionation. Resonant hard x-ray diffraction experiments on $NdNiO_3$ reveal a small asphericity of the Ni electronic states already observed above T_{MI} with little temperature dependence, which indicates that no orbital degeneracy exists in the e_g states. Therefore, orbital ordering is unlikely to occur at T_{MI} and the orbitals are possibly already ordered [10]. Resonant soft x-ray magnetic diffraction studies on $NdNiO_3$ reveal a non-collinear magnetic structure [21, 22]. This finding allows a consistent interpretation of both charge disproportionation and magnetic ordering. In this model, no up–up–down–down spin orientation is present. Neutron powder diffraction on $HoNiO_3$ supports this scenario as it is possible to described the data equally well with a collinear up–up–down–down magnetic structure as with a non-collinear magnetic structure of Ni ions [20].

In this study we present resonant soft x-ray magnetic powder diffraction on a series of $RNiO_3$ compounds with R = Pr, Nd, Eu, Ho and Y. Resonant x-ray diffraction has become a powerful technique for studying electronic and magnetic ordering phenomena in transition metal oxides. The 3d states are directly probed by the dipole 2p to 3d transitions ($L_{2,3}$ edges), leading to very strong enhancements in the scattered intensity. For most resonant magnetic x-ray diffraction studies high-quality single crystals or epitaxially grown films are required and the technique is limited to systems for which such samples are available. Pioneering work on polycrystalline samples was performed by Collins *et al* [23], exploiting the very large enhancement of the uranium M_4 edge in UO_2 where a weak magnetic diffraction peak was observed with significant effort. Kim *et al* [24] have reported on a resonant powder diffraction study in which a magnetic diffraction peak at the Gd L_2 edge in $GdNi_2Ge_2$ was observed. However, these studies were performed in the hard x-ray regime. Only very recently could we show that resonant magnetic soft x-ray powder diffraction leads to sufficiently strong signals for the study of magnetic ordering phenomena and we expanded the technique to soft x-ray resonant orbital powder diffraction [25–28].

2. Results

2.1. Experimental details and sample preparation

$RNiO_3$ compounds were prepared as polycrystalline powder by high-pressure solid state reactions, as described in the literature [6, 25, 29, 30]. Resonant soft x-ray magnetic diffraction experiments were performed with the RESOXS endstation [31] at the SIM beamline of the Swiss Light Source of the Paul Scherrer Institut, Switzerland. Polycrystalline pellets of 10 mm diameter were glued onto a copper sample holder mounted on a He flow cryostat, which achieves temperatures between 10 and 370 K. Experiments were performed using horizontal or vertical linearly polarized x-ray beams leading to π or σ incident photon polarization in the horizontal scattering geometry. Two-dimensional data sets were collected with a commercial Roper Scientific charge couple device (CCD camera) mounted in the vacuum chamber. The recorded CCD images were corrected for background (recorded at the same energy but with $\Delta 2\theta = 5°$ offset), integrated along the camera height (i.e. along the Debye–Scherrer ring) and fitted with a Lorentzian and a linear background function. This linear background originates from the fluorescence of the sample and provides a means of simultaneously recording the absorption. The obtained fluorescence spectra were normalized to literature values apart the absorption edges [32]. The recorded magnetic diffraction intensities as a function of energy have been corrected for absorption.

Properties of $RNiO_3$ with R = Pr, Nd, Eu, Ho and Y are listed in table 1, including the metal-to-insulator transition temperatures, T_{MI}, the Néel temperatures, T_N, and the tolerance factors, t.

The tolerance factor is a measure of the relative distortion of the $RNiO_3$ perovskites along the series and is defined by $t = (d_{R-O})/\sqrt{2}(d_{Ni-O})$ [29]. A variation of t is caused by the ionic radii of the R ion, i.e. increasing size of R gives rise to increasing t. The branching ratio $\sqrt{I(L_3)/(I(L_2)+I(L_3))}$,

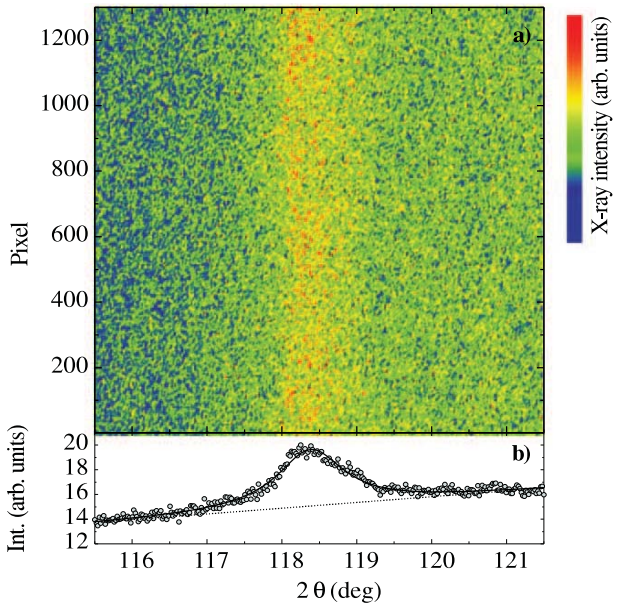

Figure 1. (a) Section of the $(\frac{1}{2}\ 0\ \frac{1}{2})$ resonant magnetic powder diffraction ring of $HoNiO_3$ at the Ni L_3 edge (853 eV) and 50 K measured with π incident light. (b) Intensity after vertical integration of the image as a function of 2θ. The solid line corresponds to a Lorentzian fit with a linear background.

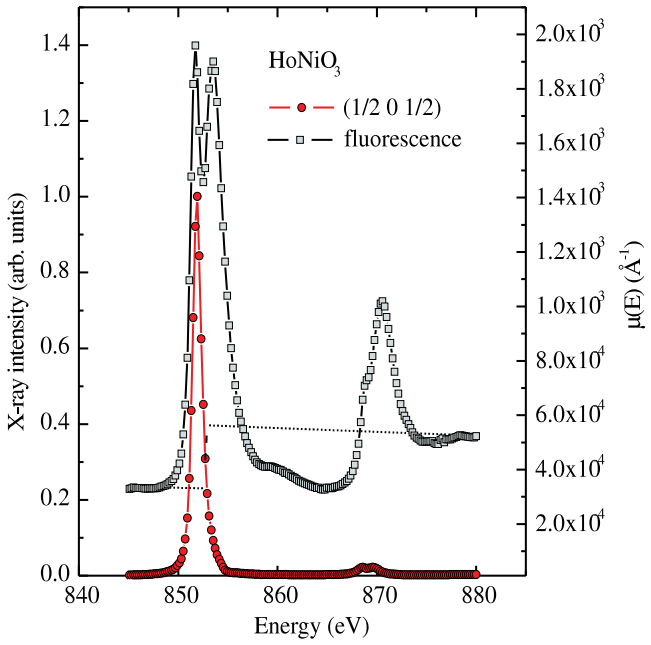

Figure 2. Energy dependence of the fluorescence and integrated intensity of the magnetic $(\frac{1}{2}\ 0\ \frac{1}{2})$ reflection of polycrystalline $HoNiO_3$ measured with π incident light at 50 K.

i.e. the square root of the ratio of integrated intensity of the L_3 peaks over that of the sum of L_2 and L_3 of $RNiO_3$, is given in table 1.

2.2. Resonant soft x-ray magnetic powder diffraction on $HoNiO_3$

Here we present a comprehensive study of resonant soft x-ray magnetic powder diffraction for the $RNiO_3$ series. Let us begin by discussing $HoNiO_3$ as an example. In the present resonant soft x-ray diffraction experiment the Ni 3d states are directly probed by 2p–3d electric dipole transitions. The resonant enhancement is so large that it leads to measurable magnetic powder diffraction intensities at the Ni $L_{2,3}$ absorption edges. An image of a section of the magnetic $(\frac{1}{2}\ 0\ \frac{1}{2})$ Debye–Scherrer diffraction ring of $HoNiO_3$ at the Ni L_3 edge (853 eV, angle of incidence $\alpha_i = 45°$) is shown in figure 1(a). A one-dimensional integration of the image leads to the magnetic $(\frac{1}{2}\ 0\ \frac{1}{2})$ reflection peak shown in figure 1(b). The integrated intensity is obtained by fitting a Lorentz function and a linear background. The linear background accounts for the simultaneously collected fluorescent radiation. The slope of the background results from unequal exposure time of the detector as there is no shutter installed, i.e. the camera is illuminated during read-out.

The energy dependence of the resonant soft x-ray scattering contains information on the electronic states of the Ni 3d shell. The energy dependence of the integrated intensity of the magnetic $(\frac{1}{2}\ 0\ \frac{1}{2})$ reflection of $HoNiO_3$ across the Ni $L_{2,3}$ edges is presented in figure 2 and compared with the simultaneously collected fluorescence radiation. The recorded magnetic $(\frac{1}{2}\ 0\ \frac{1}{2})$ diffraction data show strong resonant enhancement at the L_3 edge and weaker enhancement at the L_2 edge. While the intensity at the L_3 edge is more than one order of magnitude larger than the intensity at the L_2 edge, both edges contain two features: a narrow, intense peak at lower energy and a broad and very weak peak at higher energy. At the Ni L_3 edge the higher energy, broad peak appears only as a shoulder. At both edges the features are separated by approximately $\Delta E = 1.3 \pm 0.1$ eV from each other.

The simultaneously measured fluorescence data also show two distinct peaks at the Ni L_3 edge; a narrow intense peak at lower energy and a broad, weaker peak at high energy separated by $\Delta E = 1.8 \pm 0.1$ eV. Two features are also noticeable at the Ni L_2 edge; a main peak with a left shoulder separated by the same value as the L_3 features. The temperature dependence of the magnetic $(\frac{1}{2}\ 0\ \frac{1}{2})$ reflection taken at the maximum of the Ni L_3 edge (852 eV) is shown in figure 3. The decrease in intensity follows a typical order parameter squared behavior and disappears at the Néel temperature T_N.

2.3. Resonant soft x-ray magnetic powder diffraction on a $RNiO_3$ series

To elucidate the influence of the different R ions on the electronic structure of the Ni ions we measured the resonant magnetic diffraction of a series of $RNiO_3$ with R = Pr, Nd, Eu, Ho and Y. The selected R ions have different ionic radii (with Pr the largest and Y the smallest radius), leading to different tolerance factors and different physical properties as denoted in table 1. The obtained resonant magnetic soft x-ray diffraction data for the series in the vicinity of the Ni $L_{2,3}$ edges are presented in figure 4 and ordered according the ionic radius of the R ion. The spectra have been corrected

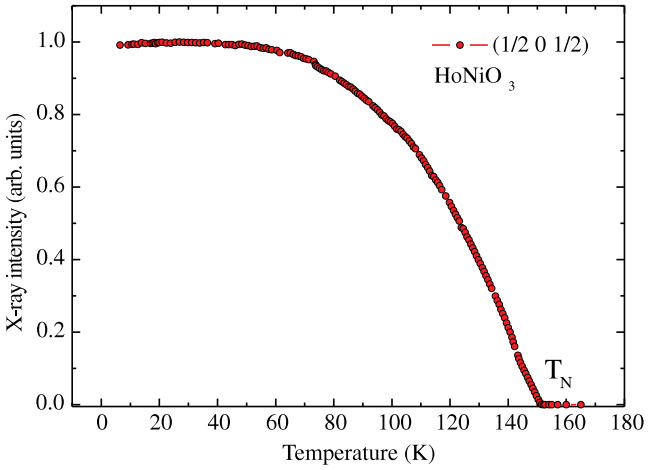

Figure 3. Temperature dependence of the integrated x-ray intensity of the magnetic ($\frac{1}{2}$ 0 $\frac{1}{2}$) reflection taken at the Ni L_3 edge at (852 eV) with π-polarized light incident on polycrystalline $HoNiO_3$. The form of this curve represents the temperature dependence of the Ni magnetic moments only.

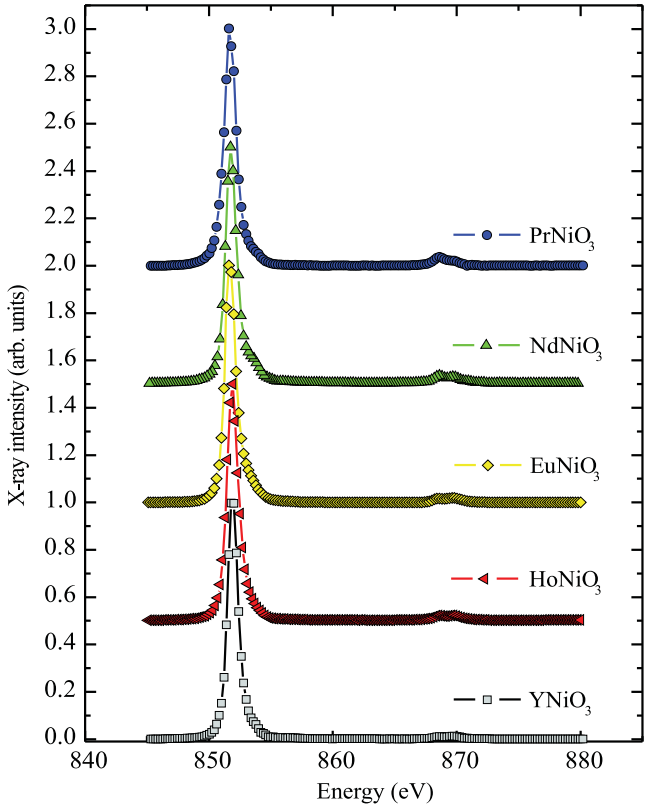

Figure 4. Energy dependence of the integrated intensity of the magnetic ($\frac{1}{2}$ 0 $\frac{1}{2}$) diffraction of polycrystalline samples of $RNiO_3$ with R = Pr, Nd, Eu, Ho and Y measured with π incident light at 50 K. The spectra are ordered with regard to increasing ionic radii of the R ion and shifted for easy comparison.

for absorption and are shifted vertically for easy comparison. As discussed above for the example of $HoNiO_3$, all spectra contain two features at both edges, but here we also observe that the right shoulder on the main intense peak at the L_3 edge becomes more pronounced with increasing radius of the R ion. The same observation holds for the L_2 edge where the left peak becomes more intense on going towards larger ionic radii within the series. Remarkably, neither peak varies in energy within the whole series. The separation in energy for both peaks is constant $\Delta E = 1.3 \pm 0.1$ eV for $RNiO_3$. The intensity ratio between the left and right peaks at the L_2 edge is observed to decrease slightly going from R = Pr to Y. While the same trend is observed at the L_3 edge, a precise analysis is difficult because of the overlap of the peaks. Apart from these small changes, the experimental spectra look very similar for all investigated compounds.

In table 1 the branching ratio $\sqrt{I(L_3)/(I(L_2)+I(L_3))}$, i.e. the square root of the ratio of integrated intensity of the L_3 peaks over that of the sum of L_2 and L_3 of $RNiO_3$, is given. While magnetic diffraction spectra are linked to magnetic circular dichroism (XMCD) through the optical theorem, magnetic diffraction spectra also scale with the square of the magnetic scattering length. Further, XMCD sum rules relate the branching ratio to the ratio of ground state spin and orbital projections $\frac{\langle S_z\rangle}{\langle L_z\rangle}$. With the assumption of zero or constant contributions of opposite sign in the integration, we find a nearly constant $\frac{\langle S_z\rangle}{\langle L_z\rangle}$ ratio, which indicates an almost constant orbital moment for the different rare earth ions in the $RNiO_3$ series.

2.4. Simulations of magnetic diffraction

Figure 5 shows the energy dependence of the ($\frac{1}{2}$ 0 $\frac{1}{2}$) reflection calculated with a charge transfer (configuration interaction) multiplet approach [35]. The upper curve in figure 5 (filled circles) represents the calculated resonant magnetic diffraction signal presented in [21] for epitaxial $NdNiO_3$ films. The parameters were chosen so that the calculation matches the experimental magnetic scattering data with the additional constraint of coincident calculated and measured absorption. The simulation includes two different Ni-sites (A, B) with mixed valence. The corresponding configuration interaction parameters are $U_{dd} - U_{pd} = -2$ eV, and the transfer integrals: $T(A_1) = T(B_1) = 2.0$ eV and $T(B_2) = T(E) = 1.3$ eV, while for Ni_A the crystal field is described by $10D_q = 1.8$ eV, $D_s = 0.1$ eV, the charge transfer $\Delta = 1.5$ eV, and for Ni_B, $10D_q = 1.5$ eV, $\Delta = -1.7$ eV. The resulting ground state of Ni_A is $\alpha_A 3d^7 + \beta_A 3d^8\mathbf{L}$ with $\alpha_A = 0.64$, $\beta_A = 0.36$ and of Ni_B $\alpha_B 3d^7 + \beta_B 3d^8\mathbf{L}$ with $\alpha_B = 0.32$, $\beta_B = 0.68$. Note that this corresponds to a valence of 2.64 for site A and 2.32 for site B. The degree of charge disproportionation is expressed by $\delta_{eff} = (1-\alpha_B) - (1-\alpha_A) = 0.32$. We analyze the influence of charge transfer on the photon energy dependence of the magnetic ($\frac{1}{2}$ 0 $\frac{1}{2}$) diffraction signal of $RNiO_3$ by increasing the Ni^{3+} percentage on Ni_A and decreasing it at Ni_B, leading to increasing charge transfer of $\delta_{eff} = 0.41$ (upper triangles); $\delta_{eff} = 0.55$ (left triangles) and $\delta_{eff} = 0.64$ for the curve with filled boxes[4]. With increasing Ni^{3+} content on site A and decreasing content on site B we

[4] The bases for the calculations are: Ni_A 70% $3d^7 + 30\%$ $3d^8\mathbf{L}$ and Ni_B 29% $3d^7 + 71\%$ $3d^8\mathbf{L}$ (upper triangles); Ni_A 77% $3d^7 + 23\%$ $3d^8\mathbf{L}$ and Ni_B 22% $3d^7 + 78\%$ $3d^8\mathbf{L}$ (left triangles); Ni_A 82% $3d^7 + 18\%$ $3d^8\mathbf{L}$ and Ni_B 18% $3d^7 + 82\%$ $3d^8\mathbf{L}$ (filled boxes).

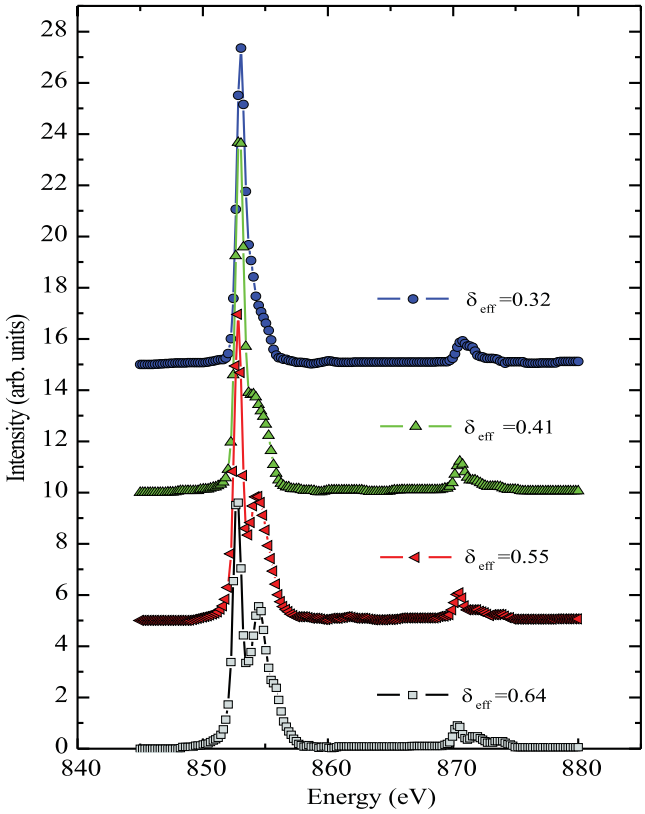

Figure 5. Calculated resonant diffraction signal for the magnetic $(\frac{1}{2}\ 0\ \frac{1}{2})$ reflection of $RNiO_3$. The different spectra are calculated with different charge disproportionation on both Ni-sites.

observe significantly increasing intensity of the right peak on both edges. Notwithstanding that we cannot assign precise numbers, a similar though less pronounced trend is observed in the measured spectra for $RNiO_3$. If charge disproportionation is indeed responsible for the changes in the measured spectra, then the change in the effective charge variation is expected to be less than $\Delta\delta_{\text{eff}} < 0.05e$ within the $RNiO_3$ series.

Further small differences in the spectrum can also be obtained by small changes in the crystal field strength. To elucidate this effect, we calculate energy spectra for different $10D_q$ values for the Ni_A- and Ni_B-sites with constant charge disproportionation $\delta_{\text{eff}} = 0.32$. In figure 6(a) we leave $10D_q$ for Ni_A constant and vary it for Ni_B and vice versa in figure 6(b). The middle curve with $10D_q(Ni_A) = 1.8$ eV and $10D_q(Ni_B) = 1.5$ eV corresponds to the upper curve in figure 5 (filled circles) and represents the calculated resonant magnetic diffraction signal presented in [21] for epitaxial $NdNiO_3$ films. A third series was calculated by varying $10D_q$ for both Ni-sites in parallel and a fourth series was calculated by varying it anti-parallel wise (data not shown). From the calculation $10D_q \geqslant 1.5$ eV for Ni_B can be estimated to be a lower limit. As shown in figure 6(a) (filled circles and upper triangle), values of $10D_q$ smaller than 1.5 eV on the Ni_B site lead to completely different spectra, with a third peak appearing on the Ni L_3 edge. We can therefore estimate an upper limit for the difference between the $10D_q$ for both sites to be $10D_q(Ni_A) - 10D_q(Ni_B) \leqslant 0.3$ eV. Another result of the calculation is that the intensity of the second peak at the L_3 edge tends to be too high compared to the experimental data. To summarize, the simulations of magnetic $(\frac{1}{2}\ 0\ \frac{1}{2})$ diffraction could successfully reproduce the observed trends in the experimental data but only when constrained in the variation of $10D_q \leqslant 10\%$ or charge disproportionation $\leqslant 0.05e$.

2.5. Polarization dependency of the magnetic diffraction signal

To verify previous findings about magnetic structure by resonant soft x-ray diffraction we measure the magnetic $(\frac{1}{2}\ 0\ \frac{1}{2})$ diffraction across the Ni $L_{2,3}$ edges for σ and π incident light for two different R ions, R = Pr and Y. The obtained spectra of $PrNiO_3$ for both incident polarizations (σ and π) have exactly the same shape, irrespective of an overall intensity scale factor (data not shown). In general, magnetic scattering is expected to be weaker when measured with σ incident radiation because no intensity in the σ–σ scattering channel is allowed. For $PrNiO_3$ the intensity for π polarized incident radiation is approximately 1.8 ± 0.1 times larger than that for σ incident radiation. For $YNiO_3$, we found (within experimental error) the same intensity ratio between π and σ polarized incident light of 1.76 ± 0.11.

The data obtained from magnetic powder diffraction originate from grains which fulfil the Bragg condition and are oriented with random azimuthal angles. These intensities contain independent information that can be utilized to test the proposed magnetic structure models. The azimuthal angle dependence for the non-zero polarization channels for the $NdNiO_3$ magnetic $(\frac{1}{2}\ 0\ \frac{1}{2})$ reflection is calculated in three steps. First, the structure factor for the magnetic unit cell is calculated. Second the orientation of the magnetic Ni moments is calculated as a function of the azimuthal angle, and finally the polarization dependence of the incident and diffracted x-rays is evaluated [36]. Concerning the non-collinear magnetic model proposed by Scagnoli *et al* [21] the magnetic moment direction could be expressed by a universal vector, $\mathbf{m}_{A,B} = [m_{A,B}\cos(\alpha_{A,B}), 0, m_{A,B}\sin(\alpha_{A,B})]$, with $m_A \approx m_B$ but $\alpha_A \approx -\alpha_B$. A, B denote the two different Ni-sites and $\alpha = 0$ is set parallel to the crystallographic a-axis. Next, two rotations are necessary: first, a rotation, $R(\beta)$, to align the crystal axis to the magnetic wavevector, $\tau = (\frac{1}{2}\ 0\ \frac{1}{2})$ (here (0,1,0) is put $\parallel$ to τ with $\beta = 125.9°$), and second, the rotation, $R(\Psi)$, represents the azimuthal angle dependence. The resulting vector, $\mathbf{z} = R(\beta)R(\Psi)\mathbf{m}$, is used to calculate the magnetic diffraction, M, for all polarization channels as function of the azimuthal angle, Ψ, with

$$M = \begin{pmatrix} 0 & z_3\sin(\theta) + z_1\cos(\theta) \\ z_3\sin(\theta) - z_1\cos(\theta) & -z_2\sin(2\theta) \end{pmatrix}$$

and the Bragg angle $\theta \approx 55.5°$. The magnetic scattering intensities are obtained by $I_{\sigma-\pi} \propto |\ z_3\sin(\theta) + z_1\cos(\theta)\ |^2$, $I_{\pi-\sigma} \propto |\ z_3\sin(\theta) - z_1\cos(\theta)\ |^2$ and $I_{\pi-\pi} \propto |\ -z_2\sin(2\theta)\ |^2$. The intensity ratio, $I_{\pi/\sigma}$, between π and σ incident radiation can be obtained by integrating $(I_{\pi-\pi}(\Psi) + I_{\pi-\sigma}(\Psi))/I_{\sigma-\pi}(\Psi)$ over the azimuthal angle. For the non-collinear magnetic structure of epitaxial $NdNiO_3$ films presented in [21], we

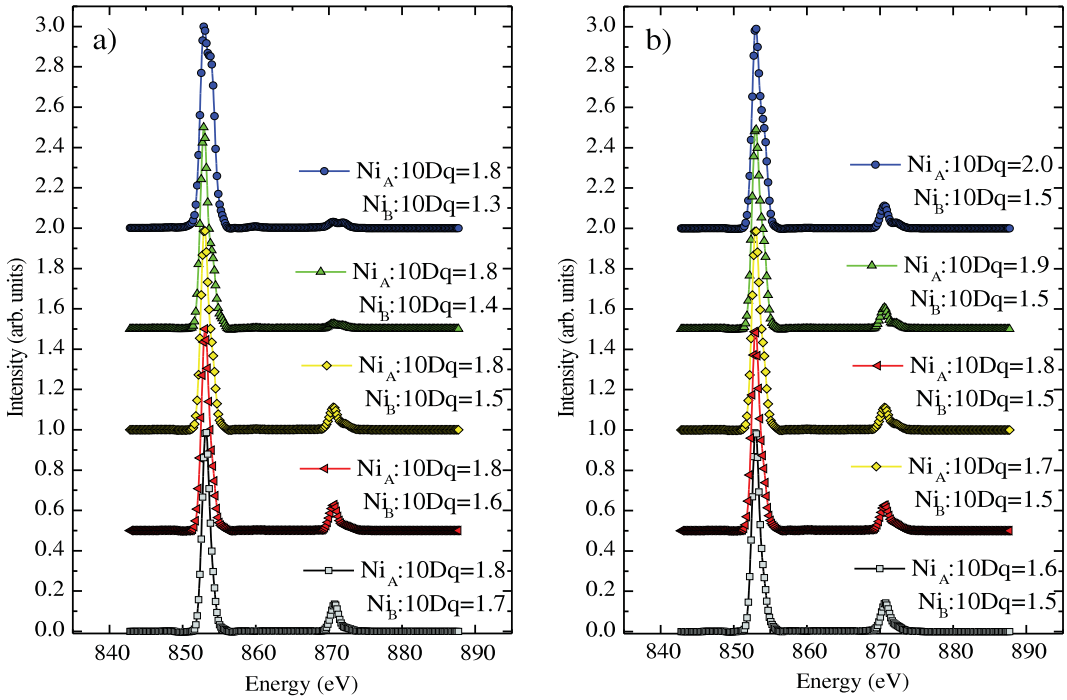

Figure 6. Calculated resonant diffraction signal for the magnetic ($\frac{1}{2}$ 0 $\frac{1}{2}$) reflection of $RNiO_3$. The different spectra are calculated with constant charge disproportionation of $\delta_{\text{eff}} = 0.32$ and different $10D_q$ for the Ni_A- and Ni_B-sites.

obtain a ratio of $I_{\pi/\sigma} = 1.7$, whereas the collinear magnetic structure [20] leads to $I_{\pi/\sigma} = 3$. Therefore, the observed ratios exclude the collinear magnetic model and suggest that $PrNiO_3$ and $YNiO_3$ possess the same non-collinear magnetic structure as $NdNiO_3$.

2.6. Absorption spectra on series of $RNiO_3$

As noted earlier, we collected fluorescence data simultaneously with the diffraction data, which are shown as a function of energy in figure 7 for $RNiO_3$ with R = Pr, Nd, Eu, Ho and Y at a temperature of 50 K. A clear splitting is observed at the L_3 edge for all compounds which are all in the insulating phase at this temperature [37]. Only small differences are noticeable among the spectra at both absorption edges. The peak intensities between the two features at the L_3 edges reverse on going from R = Pr to Y. Furthermore, the left shoulder on the L_2 edge becomes more pronounced. Absorption spectra have proven to be useful experimental probes of changes of Ni valence [38, 39]. Nevertheless, the energy position of the absorption edges depend strongly on coordination geometry, ligands and occupancies of the 3d shell. The shifts in energy for a valence change from Ni^{2+} to Ni^{4+} range from 1.4 eV (measured for pseudo-octahedral nickel dithiocarbamate and xanthate complexes) [39] to 2–3 eV predicted from electronic structure calculations [38, 40]. The absorption edge energy position of $RNiO_3$ presented in figure 7 vary within 0.6 eV for the Ni L_3 and L_2 edges for different rare earth ions. These shifts are indicative of some change in electronic structure, but they are small and so support only small changes in the electronic ground states of the different rare earth ions. Theses changes

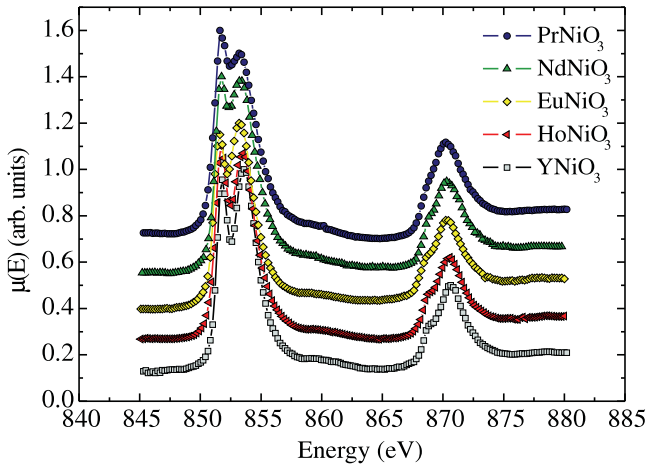

Figure 7. Ni $L_{2,3}$ absorption spectra at about 50 K for $PrNiO_3$, $NdNiO_3$, $EuNiO_3$, $HoNiO_3$ and $YNiO_3$. At 50 K all compounds are in the insulating phase.

are either connected to different $3d^n$ occupancies or to small changes in crystal field.

3. Discussion and conclusion

The present study demonstrates the capability of soft x-ray magnetic powder diffraction to extract electronic and magnetic information on transition metal oxides without the need for high-quality single crystals. We investigated a series of $RNiO_3$ perovskites with R = Pr, Nd, Eu, Ho and Y. The technique utilized enables the exploitation of fluorescence data

simultaneously with the measurement of magnetic diffraction. Spectra of the magnetic reflection show two distinct features on both edges separated by $\Delta E = 1.3 \pm 0.1$ eV. The measured magnetic diffraction signal also looks very similar for different rare earth ions, e.g. the peaks do not shift in energy, supporting only small differences in electronic structure. Apart from the very similar shape of the energy dependence of the magnetic $(\frac{1}{2}\ 0\ \frac{1}{2})$ diffraction signal a small change in the intensity ratio between the two features at both edges is also found. The same trend is reproduced by multiplet calculations by only small changes in charge disproportionation on both Ni-sites. This result is in agreement with recent studies where a slight change in charge transfer between $PrNiO_3$ and $LuNiO_3$ was found [14], but in contradiction to a recent interpretation of hard x-ray K-edge absorption spectra [18]. Distinct changes in the K absorption were detected and interpreted in terms of large changes in charge disproportionation. However, large differences in charge configuration would lead to modifications of the atomic multiplets and thus to pronounced changes in the soft x-ray magnetic diffraction and x-ray absorption spectra. A possible reason for discrepancies could be the different states probed in these processes. The hard x-ray absorption study is sensitive to the empty 4p states, which due to their spatial extension are very sensitive to the (local) crystal structure. In contrast, the soft x-rays are directly sensitive to the 3d electronic states.

Different rare earth ions lead to different local structures around the Ni ions, e.g. different Ni–O bond angles and rotation angles of the NiO_6 octahedra, resulting in different crystal field strengths. Simulations of magnetic $(\frac{1}{2}\ 0\ \frac{1}{2})$ diffraction were performed, and reproduced the observed soft x-ray spectral trends—but only when constrained to variation of $10D_q$ to 10%. From this, we conclude that the electronic structure changes remain very small within the $RNiO_3$ series, with a charge disproportionation smaller than $0.05e$ despite the strong change in T_{MI}. Further support for only small electronic changes is given by the almost constant branching ratio, indicating comparable orbital magnetic moment contributions for different rare earth ions.

A prediction on the magnetic structure of $RNiO_3$ could be made by analyzing the polarization dependence of the magnetic diffraction. We calculate the intensity ratio between π and σ incident light for the magnetic $(\frac{1}{2}\ 0\ \frac{1}{2})$ Bragg peak for the collinear and non-collinear magnetic structure. The measured ratio of $I_{\pi/\sigma}$ is clearly supportive of a non-collinear magnetic structure in $RNiO_3$. Our results emphasize that the lighter and heavier $RNiO_3$ compounds are very similar from the point of view of the local electronic and magnetic structure.

Acknowledgments

We have benefited from the experimental support of the X11MA beamline staff and help from N Stojic. The financial support of the Swiss National Science Foundation is gratefully acknowledged. MJM-L and JAA thank the Spanish Ministry of Science and Innovation for funding the Project MAT2010-16404.

References

[1] Imada M, Fujimori A and Tokura Y 1998 *Rev. Mod. Phys.* **70** 1039
[2] Lacorre P, Torrance J B, Pannetier J, Nazzal A I, Wang P W and Huang T C 1991 *J. Solid State Chem.* **91** 225
[3] Medarde M L 2007 *J. Phys.: Condens. Matter* **9** 1679
[4] Mizokawa T, Khomskii D I and Sawatzky G A 2000 *Phys. Rev.* B **61** 11263–6
[5] Mazin I I, Khomskii D I, Lengsdorf R, Alonso J A, Marshall W G, Ibberson R M, Podlesnyak A, Martínez-Lope M J and Abd-Elmeguid M M 2007 *Phys. Rev. Lett.* **98** 176406
[6] Alonso J A, García-Muñoz J L, Fernández-Díaz M T, Aranda M A G, Martínez-Lope M J and Casais M T 1999 *Phys. Rev. Lett.* **82** 3871
[7] Alonso J A, Martínez-Lope M J, Casais M T, García-Muñoz J L, Fernández-Díaz M T and Aranda M A G 2001 *Phys. Rev.* B **64** 094102
[8] Alonso J A, Martínez-Lope M J, Casais M T, García-Muñoz J L and Fernández-Díaz M T 2000 *Phys. Rev.* B **61** 1756
[9] Staub U, Meijer G I, Fauth F, Allenspach R, Bednorz J G, Karpinski J, Kazakov S M, Paolasini L and d'Acapito F 2002 *Phys. Rev. Lett.* **88** 126402
[10] Scagnoli V, Staub U, Janousch M, Mulders A M, Shi M, Meijer G I, Rosenkranz S, Wilkins S B, Paolasini L, Karpinski J, Kazakov S M and Lovesey S W 2005 *Phys. Rev.* B **72** 155111
[11] Zaghrioui M, Bulou A, Lacorre P and Laffez P 2001 *Phys. Rev.* B **64** 081102(R)
[12] Scagnoli V, Staub U, Janousch M, Meijer G I, Paolasini L, DAcapito F, Bednorz J G and Allenspach R 2004 *J. Magn. Magn. Mater.* **420** 272–6
[13] Acosta-Alejandro M, de León J M, Medarde M, Lacorre P, Konder K and Montano P A 2008 *Phys. Rev.* B **77** 085107
[14] Medarde M, Fernández-Díaz M T and Lacorre P 2008 *Phys. Rev.* B **78** 212101
[15] van den Brink J and Khomskii D I 2008 *J. Phys.: Condens. Matter* **20** 434217
[16] Cheong S W and Mostovoy M 2007 *Nat. Mater.* **6** 13–20
[17] Giovannetti G, Kumar S, Khomskii D, Picozzi S and van den Brink J 2009 *Phys. Rev. Lett.* **103** 156401
[18] Medarde M, Dallera C, Grioni M, Delley B, Vernay F, Mesot J, Sikora M, Alonso J A and Martínez-Lope M J 2009 *Phys. Rev.* B **80** 245105
[19] García-Muñoz J L, Rodríguez-Carvajal J and Lacorre P 1992 *Europhys. Lett.* **20** 241
[20] Fernández-Díaz M T, Alonso J A, Martínez-Lope M J, Casais M T and García-Muñoz J L 2001 *Phys. Rev.* B **64** 144417
[21] Scagnoli V, Staub U, Mulders A M, Janousch M, Meijer G I, Hammerl G, Tonnerre J M and Stojic N 2006 *Phys. Rev.* B **73** 100409(R)
[22] Scagnoli V, Staub U, Bodenthin Y, García-Fernández M, Mulders A M, Meijer G I and Hammerl G 2008 *Phys. Rev.* B **77** 115138
[23] Collins S P, Laundy D, Tang C C and Cernik R J 1995 *J. Phys.: Condens. Matter* **7** L223
[24] Kim J W, Tan L, Budko D W S L, Canfield P C and Goldman A 2005 *J. Phys.: Condens. Matter* **17** L493
[25] Staub U, García-Fernández M, Mulders A M, Bodenthin Y, Martínez-Lope M J and Alonso J A 2007 *J. Phys.: Condens. Matter* **19** 092201
[26] García-Fernández M, Staub U, Bodenthin Y, Lawrence S M, Mulders A M, Buckley C E, Weyeneth S, Pomjakushina E and Conder K 2008 *Phys. Rev.* B **77** 060402(R)
[27] Staub U, García-Fernández M, Bodenthin Y, Scagnoli V, Souza R A D, Garganourakis M, Pomjakushina E and Conder K 2009 *Phys. Rev.* B **79** 224419

[28] García-Fernández M, Staub U, Bodenthin Y, Scagnoli V, Pomjakushin V, Lovesey S W, Mirone A, Herrero-Martín J, Piamonteze C and Pomjakushina E 2009 *Phys. Rev. Lett.* **103** 097205
[29] Alonso J A, Martínez-Lope M J, Casais M T, Aranda M A G and Fernández-Díaz M T 1999 *J. Am. Chem. Soc.* **121** 4754
[30] Alonso J A, Martínez-Lope M J and Rasines I J 1995 *Solid State Chem.* **120** 170
[31] Staub U, Scagnoli V, Bodenthin Y, García-Fernández M, Wetter R, Mulders A M, Grimmer H and Horisberger M 2008 *J. Synchrotron Radiat.* **15** 469
[32] Henke B L, Gullikson E M and Davis J C 1993 *At. Data Nucl. Data Tables* **54** 181–342
[33] Torrance J B, Lacorre P, Nazzal A I, Ansaldo E J and Niedermayer C 1992 *Phys. Rev.* B **45** 8209
[34] García-Muñoz J L, Rodríguez-Carvajal J, Lacorre P and Torrance J B 1992 *Phys. Rev.* B **46** 4414
[35] de Groot F M F 2005 *Coord. Chem. Rev.* **249** 31
[36] Hill J P and McMorrow D F 1996 *Acta Crystallogr.* A **52** 236
[37] Piamonteze C, de Groot F M F, Tolentino H C N, Ramos A Y, Massa N E, Alonso J A and Martínez-Lope M J 2005 *Phys. Rev.* B **71** 020406(R)
[38] Miao S, Kocher M, Rez P, Fultz B, Ozawa Y, Yazami R and Ahn C C 2005 *J. Phys. Chem.* B **109** 23473
[39] Collison D, Garner C D, McGrath C M, Mosselmans J F W, Pidcock E, Roper M D, Searle B G, Seddon J M W, Sinn E and Young N A 1988 *J. Chem. Soc. Dalton Trans.* 4179
[40] van der Laan G and Kirkman I W 1992 *J. Phys.: Condens. Matter* **4** 4189